Dyes and Pigments 180 (2020) 108451

Contents lists available at ScienceDirect

Dyes and Pigments

journal homepage: http://www.elsevier.com/locate/dyepig

# Vapor-, thermo-, and mechanical-grinding-triggered tri-stimuli-responsive luminescence switching of cycloplatinated(II) complex bearing 8-quinolinol derivatives

Jun Ni *, Gao Liu, Mengmeng Su, Wei Zheng, Jianjun Zhang

*College of Chemistry, Dalian University of Technology, Linggong Road No. 2, Dalian, 116024, PR China*

ARTICLE INFO

*Keywords:*
Cycloplatinated(II) complex
Near-infrared
Vapoluminescence
Thermochromic luminescence
Mechanoluminescence
Tri-stimuli-responsive

ABSTRACT

Four novel cycloplatinated(II) complexes, Pt(ppy)(L1) (**1**), Pt(ppy)(L2) (**2**), Pt(ppy)(L3) (**3**) and Pt(ppy)(L4) (**4**) based on 5-[2-(4-substituent-phenyl)ethynyl]-8-quinolinol ligands {substituent = H (L1), Me(L2), Et(L3), $^{t}$Bu (L4)} were synthesized and characterized. Complex **4** has three main pseudopolymorphs, including orange **4**·$CH_3CH_2OH$, red **4R**, and dark-brown **4**·½($CCl_4$). Complex **4** exhibits interesting tri-stimuli-responsive luminescence switching properties. Upon exposure to different VOC vapors, three pseudopolymorphs display unusual irreversible vapoluminescence that **4R** and **4**·½ ($CCl_4$) can be exchanged with each other and be irreversibly converted to **4**·$CH_3CH_2OH$. Furthermore, **4**·½($CCl_4$) shows reversible thermochromic luminescence behaviour and can be reversibly converted to **4R** upon heating. No detectable change in color and luminescence of **4**·$CH_3CH_2OH$ and **4R** can be found during the heating process, although **4**·$CH_3CH_2OH$ lost its solvent and changed to desolvated **4O**. In addition, **4**·$CH_3CH_2OH$, and **4**·½ ($CCl_4$) also show the mechanoluminescent property that both of them will be converted to the same red amorphous **4G** peaked at 742 nm after grinding. Systematic studies revealed that the tri-stimuli-responsive luminescence switching property of **4** is due to the structural conversion and resultant changes of the lowest-energy excited states. In contrast, complexes **1–3** have not any luminescent switching property. The reason is most likely due to the compact stacking structures of them which prevent their structural conversion triggered by external stimuli.

## 1. Introduction

Square-planar Pt(II) complexes have attracted great attention due to their various applications, such as organic light-emitting diodes(OLEDs) [1–5], light-harvesting devices [6–8], display devices [9–12], and bio-imaging probes [13–16]. The unique square-planar geometry and a vacant coordination site of Pt(II) center allow the axial substrate-binding interactions of Pt(II) complexes, which make them conducive to the formation of different aggregates through intermolecular Pt-Pt interactions, resulting in decrease of the energy gaps between HOMO and LUMO and increase of emission wavelength [17–20]. In addition, their rich excited state energy levels are very sensitive to the conversion of stacking structures and resultant changes of intermolecular interactions such as Pt-Pt contact, hydrogen bonding, or aromatic π-π stacking caused by external stimulus [21–28]. These characteristics make square-planar Pt(II) complexes have versatile luminescence switching behaviour and exhibit important application value in phosphorescence sensors devices and data security storage [29–37].

Cycloplatinated(II) complexes are a very important part of square-planar Pt(II) complex. They exhibit high-efficiency phosphorescence caused by strong ligand-field effects and spin-orbit coupling and show a wide application prospects in the fields of high efficiency light-emitting or electroluminescence devices [38–43], photo-catalysis [44–46] and photooxidation systems [47–49]. As one of the most famous ligands, 2-phenylpyridine (ppy) derivatives have been successfully used to prepare different kinds of cycloplatinated(II) complexes by combining with other bidentate auxiliary ligands such as *β*-diketonate, 8-quinolinol, and 2-carboxypyridine [50–58]. However, compared with diimine platinum (II) complexes, the research on cycloplatinated(II) complex is still not deep enough neither in the number of complex nor in the theory and application. For example, no more than 30 platinum(II) complexes based on both 2-phenylpyridine and 8-quinolinol derivatives have been reported up until now [55–65]. Furthermore, although cycloplatinated (II) complexes also have the square-planar structure, the luminescence

* Corresponding author.
*E-mail address:* nijun@dlut.edu.cn (J. Ni).

https://doi.org/10.1016/j.dyepig.2020.108451
Received 13 March 2020; Received in revised form 14 April 2020; Accepted 14 April 2020
Available online 20 April 2020

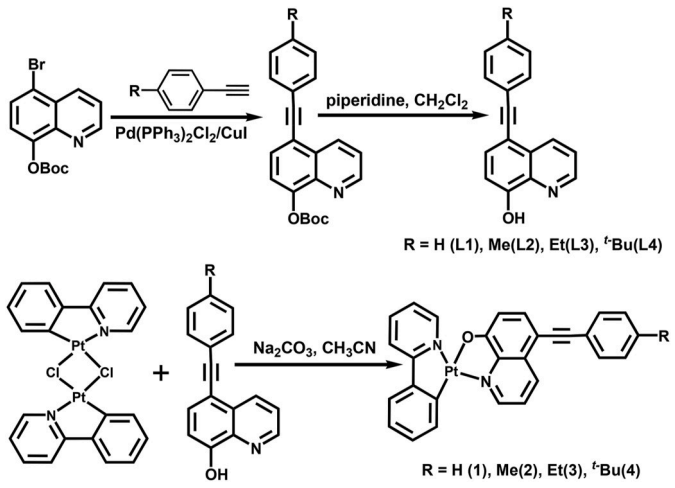


**Scheme 1.** Synthetic routes of ligands **L1-L4** and complexes **1**–**4**.

switching property of them was seldom studied. Thus, the preparation of new cycloplatinated(II) complexes and in-depth studied of their properties are very important and necessary for better understanding and practical application of such materials.

Our research interests focus on the luminescence switching property and application of Pt(II) complexes [20,23,36,66–68]. Recently, we reported a series of cycloplatinated(II) complexes with ppy and $\beta$-diketonate derivatives [68]. These complexes exhibited mechanoluminescence and concentration-dependent luminescence switching properties caused by the molecular aggregation. As a continuation of our research work, we report here the syntheses, structures and luminescence switching properties of four new cycloplatinated(II) complexes, Pt(ppy)(L) (**1–4**) {where L = 5-[2-(4-substituent-phenyl)ethynyl]-8-quinolinol; substituent = H(**L1**), Me(**L2**), Et(**L3**), and $^t$Bu(**L4**)}, bearing 2-phenylpyridine ligand and 8-quinolinol derivatives (Scheme 1). Among them, complex **4** has three main pseudopolymorphs, including orange **4**·$CH_3CH_2OH$, red **4R**, and dark-brown **4**·½($CCl_4$), which exhibit vapor-, thermo-, and mechanical-grinding-triggered tri-stimulus-responsive color and luminescence switching properties. In contrast, **1–3** have not any luminescence switching property. Systematic studies on the crystal structure, luminescence spectra, TGA, and PXRD revealed that the tri-stimulus-responsive luminescence switching properties of **4** is due to the structural conversion and resultant changes of the lowest-energy excited states. In contrast, **1–3** have not any luminescence switching property which is most likely due to their compact stacking structure that prevents the structural conversion triggered by external stimuli. Interestingly, the dark-brown **4**·½($CCl_4$) exhibits a near-infrared (NIR) luminescence peaked at 808 nm. As far as we know, it is first Pt(II) complex based on 8-quinolinol derivatives that emits more than 800 nm in solid state.

## 2. Experimental section

### 2.1. Regent and materials

All reactions were protected by a dry argon. Intermediate di-$\mu$-chlorobis[2-(2-pyridinyl-κN)-phenyl-κC]di-platinum [$Pt_2(ppy)_2(\mu\text{-}Cl)_2$] was prepared by the literature method [69]. The ligands, 5-(2-Phenylethynyl)-8-quinolinol (L1), 5-[2-(4-Methylphenyl)ethynyl]-8-quinolinol (L2), 5-[2-(4-Ethylphenyl)ethynyl]-8-quinolinol (L3), and 5-[2-(4-Ethylphenyl)ethynyl]-8-quinolinol (L4) were prepared by similar method according to the reported procedure [70]. All other reagents were purchased from commercial sources and used as received.

### 2.2. Synthetic procedures

#### 2.2.1. General method for the preparation of *L1-L4*

A solution of 5-Bromo-8-tert-butoxycarbonyloxyquinoline (1.0 g, 3.09 mmol), the phenylacetylene derivatives (3.09 mmol), and diisopropylamine (30 mL) in THF (30 mL) was purged with argon for 15 min at room temperature. Then a solid mixture of $Pd(PPh_3)_2Cl_2$ (140 mg, 0.2 mmol) and CuI (38 mg, 0.2 mmol) was added under argon atmosphere and the mixture was stirred at 60 °C overnight. The reaction mixture was filtered and washed with THF (30 mL). The filtrate was concentrated under vacuum and the pure Boc derivatives were obtained by silica gel chromatography using petroleum ether and ethyl acetate (V/V = 10:1) as the eluent.

To a 30 mL dry $CH_2Cl_2$ solution of above obtained Boc derivatives, piperidine (about 3 equiv) was added and the reaction mixture was stirred for 2 h at room temperature. Then, the solvent was removed under vacuum and the pure products were obtained by silica gel chromatography using $CH_2Cl_2$ as the eluent.

*2.2.1.1. 5-(2-phenylethynyl)-8-quinolinol **(L1)**.* Phenylacetylene was used as the starting acetylene derivative. Yield: 409 mg (54%) of a yellowish powder. M.p. 139–142 °C. ESI-MS *m/z* calculated for [$M^+$] 245.2, found 245.1. $^1$H NMR (400 MHz, $CDCl_3$, ppm): $\delta$ 8.840 (d, $J$ = 4.0 Hz, 1H), 8.716 (d, $J$ = 8.0 Hz, 1H), 7.750 (d, $J$ = 8.0 Hz, 1H), 7.571–7.622 (m, 3H), 7.365–7.408 (m, 3H), 7.196 (d, $J$ = 8.0 Hz, 1H). $^{13}$C NMR (100 MHz, $CDCl_3$, ppm): $\delta$ 155.76, 152.72, 148.34, 138.12, 135.20, 132.97, 131.99, 128.92, 122.68, 115.86, 114.37, 111.94, 109.98, 92.65, 85.33. Elem. Anal.: $C_{17}H_{11}NO$ (%) Calcd for: C, 83.25; H, 4.52; N, 5.71. Found (%): C, 83.24; H, 4.54; N, 5.73.

*2.2.1.2. 5-[2-(4-methylphenyl)ethynyl]-8-quinolinol **(L2)**.* 4-Methylphenylacetylene was used as the starting acetylene derivative. Yield: 464 mg (58%) of a yellowish powder. M.p. 147–150 °C. ESI-MS *m/z* calculated for [$M^+$] 259.3, found 259.5. $^1$H NMR (400 MHz, DMSO-$d_6$, ppm): $\delta$ 8.939 (d, $J$ = 4.0 Hz, 1H), 8.658 (d, $J$ = 7.2 Hz, 1H), 7.701–7.740 (m, 2H), 7.547 (d, $J$ = 7.2 Hz, 2H), 7.263 (d, $J$ = 7.2 Hz, 2H), 7.109 (d, $J$ = 7.2 Hz, 1H), 2.359 (s, 3H). $^{13}$C NMR (100 MHz, $CDCl_3$, ppm): $\delta$ 159.69, 152.60, 148.24, 138.04, 135.17, 132.99, 131.98, 128.84, 122.40, 115.46, 114.12, 111.77, 109.93, 92.76, 85.00, 29.71. Elem. Anal.: $C_{18}H_{13}NO$ (%) Calcd for: C, 83.37; H, 5.05; N, 5.40. Found (%): C, 83.34; H, 5.06; N, 5.38.

*2.2.1.3. 5-[2-(4-ethylphenyl)ethynyl]-8-quinolinol **(L3)**.* 4-Ethyl-phenylacetylene was used as the starting acetylene derivative. Yield: 472 mg (56%) of a yellowish powder. M.p. 178–181 °C. ESI-MS *m/z* calculated for [$M]^+$ 273.3, found 273.2. $^1$H NMR (400 MHz, DMSO-$d_6$, ppm): $\delta$ 8.942 (d, $J$ = 3.2 Hz, 1H), 8.666 (d, $J$ = 3.2 Hz, 1H), 7.732 (d, $J$ = 6.4 Hz, 1H), 7.708 (t, $J$ = 3.2 Hz, 1H), 7.573 (d, $J$ = 6.4 Hz, 2H), 7.292 (d, $J$ = 6.4 Hz, 2H), 7.112 (d, $J$ = 6.4 Hz, 1H), 2.634 (q, $J$ = 6.0 Hz, 2H), 1.192 (t, $J$ = 6.0 Hz, 3H). $^{13}$C NMR (100 MHz, $CDCl_3$, ppm): $\delta$ 154.98, 152.77, 148.27, 138.04, 135.12, 132.13, 131.51, 128.03, 122.91, 122.42, 120.51, 111.63, 109.95, 93.01, 85.69, 31.94, 15.39. Elem. Anal.: $C_{19}H_{15}NO$ (%) Calcd for: C, 83.49; H, 5.53; N, 5.12. Found (%): C, 83.47; H, 5.56; N, 5.55.

*2.2.1.4. 5-[2-(4-tert-butylphenyl)ethynyl]-8-quinolinol **(L4)**.* 4-*tert*-butyl-phenylacetylene was used as the starting acetylene derivative. Yield: 472 mg (56%) of a yellowish powder. M.p. 176–178 °C. ESI-MS *m/z* calculated for [$M^+$] 301.4, found 301.3. $^1$H NMR (400 MHz, DMSO-$d_6$, ppm): $\delta$ 8.939 (d, $J$ = 4.0 Hz, 1H), 8.655 (d, $J$ = 8.0 Hz, 1H), 7.708–7.749 (m, 2H), 7.584 (d, $J$ = 6.8 Hz, 2H), 7.467 (d, $J$ = 6.8 Hz, 2H), 7.107 (d, $J$ = 6.8 Hz, 1H), 1.234 (s, 9H). $^{13}$C NMR (100 MHz, $CDCl_3$, ppm): $\delta$ 152.72, 151.66, 148.23, 138.01, 135.18, 132.17, 131.27, 128.90, 125.47, 122.44, 120.30, 111.65, 109.94, 92.95, 85.68, 34.84, 31.90. Elem. Anal.: $C_{21}H_{19}NO$ (%) Calcd for: C, 83.69; H, 6.35; N, 4.65.

Found (%): C, 83.70; H, 6.51; N, 4.65.

#### 2.2.2. General method for the preparation of complex **1-4**

$Pt_2(ppy)_2(\mu\text{-}Cl)_2$ (385 mg, 0.50 mmol), 8-quinolinol ligands (1 mmol), and $Na_2CO_3$ (530 mg, 5 mmol) were added to $CH_3CN$ (30 mL) and the reaction mixture was stirred for 18 h at room temperature. Then, the solvent was removed under vacuum and the pure products were obtained by silica gel chromatography using $CH_2Cl_2$ as the eluent.

##### 2.2.2.1. *[5-(2-phenylethynyl)-8-quinolinolato-κ$N^1$,κ$O^8$][2-(2-pyridinyl-κN)phenyl-κC]platinum(II)* ***(1)***.

Yield: 552 mg (93%) of a red powder. M.p.: >250 °C. IR (neat, $cm^{-1}$): 3066 (w), 2961(s), 2915(s), 2851(s), 2200 (m), 1610(w), 1578(s), 1552(m), 1506(m), 1485(s), 1464(s), 1382(m), 1336(s), 1258(s), 1196(w), 1096(s), 1007(s), 911(w), 868(w), 795(s), 756(s), 728(s), 686(s). HRMS (*m/z*): calcd for $C_{28}H_{18}N_2OPt$: 593.1067, found: 593.1058 $[M]^+$. $^1H$ NMR (400 MHz, DMSO-$d_6$, ppm): $\delta$ 9.413 (d, $J$ = 4.4 Hz, 1H), 9.255 (d, $J$ = 4.4 Hz, 1H), 8.946 (d, $J$ = 6.0 Hz, 1H), 8.104 (dd, $J$ = 12.0, 6.0 Hz, 2H), 7.883 (dd, $J$ = 6.0, 4.4 Hz, 1H), 7.789 (dd, $J$ = 6.0, 4.0 Hz, 2H), 7.659–7.686 (m, 3H), 7.410–7.506 (m, 4H), 7.271 (t, $J$ = 4.0 Hz, 1H), 7.172 (t, $J$ = 4.0 Hz, 1H), 6.983 (d, $J$ = 6.0 Hz, 1H). $^{13}C$ NMR (100 MHz, $CDCl_3$, ppm): $\delta$ 168.20, 167.12, 149.52, 147.80, 146.72, 146.34, 138.95, 138.83, 137.83, 137.56, 135.21, 131.98, 131.81, 131.35, 129.61, 128.41, 127.87, 124.03, 123.70, 121.70, 121.61, 118.28, 116.06, 104.70, 92.36, 86.85. Elem. Anal.: $C_{28}H_{18}N_2OPt$ (%) Calcd for: C, 56.66; H, 3.06; N, 4.72. Found (%): C, 56.67; H, 3.06; N, 4.71. UV/Vis ($CH_2Cl_2$) $\lambda_{max}$ nm (log $\varepsilon$): 480 (3.676), 358 (3.802), 316 (4.216), 265 (4.487), 227 (4.762).

##### 2.2.2.2. *[5-(2-(4-methylphenyl)ethynyl)-8-quinolinolato-κ$N^1$,κ$O^8$][2-(2-pyridinyl-κN)phenyl-κC] platinum(II)* ***(2)***.

Yield: 559 mg (92%) of a red powder. M.p.: >250 °C. IR (neat, $cm^{-1}$): 3064 (w), 2961(s), 2924(s), 2855(s), 2200(m), 1609(s), 1585(s), 1559(m), 1501(m), 1481(m), 1463 (s), 1404(m), 1334(s), 1295(m), 1265(m), 1234(m), 1165(w), 1116(w), 1100(s), 1016(w), 989(m), 827(s), 775(s), 748(s), 706(s). HRMS (*m/z*): calcd for $C_{29}H_{20}N_2OPt$: 607.1224, found: 607.1234 $[M]^+$. $^1H$ NMR (400 MHz, DMSO-$d_6$, ppm): $\delta$ 9.046 (d, $J$ = 4.8 Hz, 1H), 9.253 (d, $J$ = 4.8 Hz, 1H), 8.926 (d, $J$ = 6.0 Hz, 1H), 8.100 (dd, $J$ = 12.0, 6.0 Hz, 2H), 7.874 (dd, $J$ = 6.0, 4.0 Hz, 1H), 7.770 (t, $J$ = 6.0 Hz, 2H), 7.670 (d, $J$ = 6.0 Hz, 1H), 7.543 (d, $J$ = 6.0 Hz, 2H), 7.480 (t, $J$ = 4.0 Hz, 1H), 7.258–7.293 (m, 3H), 7.168 (t, $J$ = 6.0 Hz, 1H), 6.973 (d, $J$ = 6.0 Hz, 1H), 2.361 (s, 3H). $^{13}C$ NMR (100 MHz, $CDCl_3$, ppm): $\delta$ 168.19, 167.10, 149.46, 147.70, 146.65, 146.27, 138.98, 138.78, 137.94, 137.70, 134.96, 131.88, 131.76, 131.24, 129.52, 129.18, 123.96, 123.57, 121.62, 121.50, 120.76, 118.17, 115.98, 104.86, 92.45, 86.17, 21.54. Elem. Anal.: $C_{29}H_{20}N_2OPt$ (%) Calcd for: C, 57.33; H, 3.32; N, 4.61. Found (%): C, 57.34; H, 3.31; N, 4.60. UV/Vis ($CH_2Cl_2$) $\lambda_{max}$ nm (log $\varepsilon$): 498 (3.750), 358 (3.818), 316 (4.277), 271 (4.503), 229 (4.831).

##### 2.2.2.3. *[5-(2-(4-ethylphenyl)ethynyl)-8-quinolinolato-κ$N^1$,κ$O^8$][2-(2-pyridinyl-κN)phenyl-κC] platinum(II)* ***(3)***.

Yield: 566 mg (91%) of a red powder. M.p.: >250 °C. IR (neat, $cm^{-1}$): 3071 (w), 2955(s), 2917(s), 2850(s), 2206(m), 1606(s), 1585(s), 1562(m), 1496(m), 1463(s), 1384 (m), 1324(s), 1285(m), 1265(m), 1242(s), 1167(m), 1131(m), 1104(m), 1084(s), 1024(m), 943(w), 821(s), 766(s), 731(s). HRMS (*m/z*): calcd for $C_{30}H_{22}N_2OPt$: 621.1380, found: 621.1361 $[M]^+$. $^1H$ NMR (400 MHz, DMSO-$d_6$, ppm): $\delta$ 9.393 (d, $J$ = 2.8 Hz, 1H), 9.241 (d, $J$ = 5.2 Hz, 1H), 8.913 (d, $J$ = 6.8 Hz, 1H), 8.088 (dd, $J$ = 13.2, 6.0 Hz, 2H), 7.860 (t, $J$ = 5.2 Hz, 1H), 7.766–7.787 (m, 2H), 7.662 (d, $J$ = 6.0 Hz, 1H), 7.563 (d, $J$ = 6.4 Hz, 2H), 7.467 (t, $J$ = 4.8 Hz, 1H), 7.285 (d, $J$ = 6.4 Hz, 2H), 7.260 (d, $J$ = 6.4 Hz, 1H), 7.164 (t, $J$ = 6.0 Hz, 1H), 6.965 (d, $J$ = 6.4 Hz, 1H), 2.636 (q, $J$ = 6.0 Hz, 2H), 2.361 (t, $J$ = 6.0 Hz, 3H). $^{13}C$ NMR was not measured due to low solubility of this complex in common NMR solvents. Elem. Anal.: $C_{30}H_{22}N_2OPt$ (%) Calcd for: C, 57.97; H, 3.57; N, 4.51. Found (%): C, 57.94; H, 3.56; N, 4.50. UV/Vis ($CH_2Cl_2$) $\lambda_{max}$ nm (log $\varepsilon$): 500 (3.773), 359 (3.815), 316 (4.318), 271 (4.476), 229 (4.752).

##### 2.2.2.4. *[5-(2-(4-tert-butylphenyl)ethynyl)-8-quinolinolato-κ$N^1$,κ$O^8$][2-(2-pyridinyl-κN)phenyl-κC] platinum(II)* ***(4)***.

Yield: 585 mg (90%) of a red powder. M.p.: >250 °C. IR (neat, $cm^{-1}$): 3064 (w), 2961(s), 2924(s), 2855(s), 2200(m), 1605(s), 1578(s), 1559(s), 1501(s), 1481(m), 1463 (s), 1404(s), 1334(s), 1295(m), 1265(m), 1234(m), 1165(w), 1116(w), 1100(s), 989(m), 827(s), 775(s), 748(s), 706(s). HRMS (*m/z*): calcd for $C_{29}H_{20}N_2OPt$: 607.1224, found: 607.1234 $[M]^+$. $^1H$ NMR (400 MHz, DMSO-$d_6$, ppm): $\delta$ 9.428 (d, $J$ = 5.2 Hz, 1H), 9.275 (d, $J$ = 5.2 Hz, 1H), 8.942 (d, $J$ = 6.8 Hz, 1H), 8.124 (dd, $J$ = 12.0, 6.0 Hz, 2H), 7.900 (dd, $J$ = 6.8, 4.0 Hz, 1H), 7.800–7.825 (m, 2H), 7.692 (d, $J$ = 6.8 Hz, 1H), 7.600 (d, $J$ = 6.0 Hz, 2H), 7.484–7.527 (m, 3H), 7.288 (t, $J$ = 6.0 Hz, 1H), 7.190 (t, $J$ = 6.0 Hz, 1H), 6.966 (d, $J$ = 6.0 Hz, 1H), 1.337 (s, 9H). $^{13}C$ NMR (100 MHz, $CDCl_3$, ppm): $\delta$ 168.19, 167.09, 151.14, 149.45, 147.69, 146.66, 146.26, 138.99, 138.77, 137.69, 134.97, 131.91, 131.76, 131.10, 129.51, 125.42, 123.96, 123.56, 121.61, 121.50, 120.82, 118.16, 115.95, 104.87, 92.40, 86.19, 34.81, 31.25. Elem. Anal.: $C_{32}H_{26}N_2OPt$ (%) Calcd for: C, 59.16; H, 4.03; N, 4.31. Found (%): C, 59.14; H, 4.01; N, 4.30. UV/Vis ($CH_2Cl_2$) $\lambda_{max}$ nm (log $\varepsilon$): 503 (3.890), 359 (3.927), 321 (4.348), 272 (4.466), 229 (4.703).

### 2.3. Measurements

Infrared (IR) spectra were measured on Nicolet 6700 FT-IR spectrophotometer, while Bruker Advance II (400 MHz) spectrometer provided the $^1H$ NMR and $^{13}C$ NMR spectra. Thermogravimetric analysis (TGA) was performed under the $N_2$ atmosphere using a TA-Q50 thermogravimetric analyzer with a heating rate of 10 °C/min. Differential scanning calorimetry (DSC) was performed under the $N_2$ atmosphere at a heating rate of 5 °C/min in a TA Instrument Q20 Differential Scanning Calorimeter. Electrospray ionization mass spectra (ESI-MS) was performed on A Finnigan LCQ mass spectrometer. UV–vis absorption spectra was acquired from PerkinElmer Lambda 25 UV–vis spectrometer. Powder X-ray diffraction (PXRD) were measured on a D/MAX-2400 with the scan rate of 4°/min. Elemental analysis of C, H and N were performed on a PerkinElmer model 240 C elemental analyzer. Luminescent properties were measured on the PerkinElmer LS55 luminescence spectrometer with a red-sensitive photomultiplier type R928 and Edinburgh analytical instrument (F920 fluorescence spectrometer). Emission lifetimes in solid states and degassed solutions were determined using an Edinburgh analytical instrument (F920 fluorescence spectrometer). The emission quantum yield ($\Phi_{em}$) in degassed dichloromethane solution at room temperature was calculated by $\Phi_s = \Phi_r(B_r/B_s)(n_s/n_r)^2(D_s/D_r)$ using $[Ru(bpy)_3](PF_6)_2$ in degassed acetonitrile as the standard ($\Phi_{em}$ = 0.062), where the subscripts 'r' and 's' denote reference standard and the sample solution, respectively, and $n$, $D$, and $\Phi$ are the refractive index of the solvents, the integrated intensity, and the luminescence quantum yield, respectively. The quantity $B$ is calculated by $B = 1–10^{-AL}$, where $A$ is the absorbance at the excitation wavelength and $L$ is the optical path length. Absolute quantum yields of complexes in solid state were determined in air by an integrating sphere (142 mm in diameter) using an Edinburgh FLS920 spectrofuorophotometer.

### 2.4. X-ray crystallography

Crystal of **1** was obtained by diffusing petroleum ether onto its dichloromethane solution. The data of crystal was collected on a Bruker SMART APEX II CCD area detector system. Structure was solved using direct methods and refined by a full-matrix least-squares methods procedure on $F^2$ with anisotropic thermal parameters for all non-hydrogen atoms using the SHELXTL–97 program package [71,72]. Table S1 of the Supporting Information gives the detailed crystallographic data and structure refinement parameters.

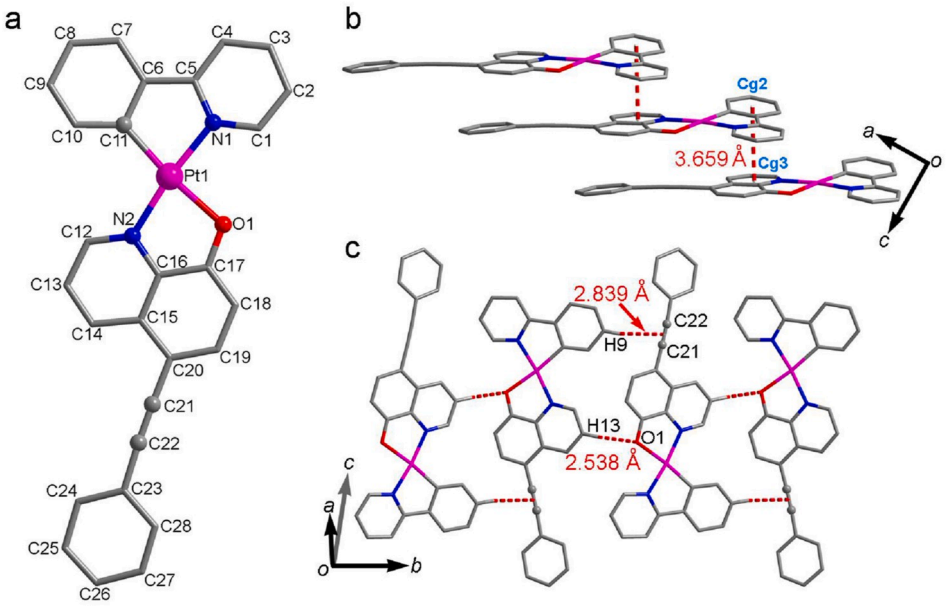


**Fig. 1.** The molecular structure (a), 1-D scalene cylinder structure (b), and interactions between adjacent molecules along *b* axis (c) of complex **1**.

## 3. Results and discussion

### 3.1. Preparation and structures

Complexes **1–4** were prepared in high yields by the reaction of the precursor $Pt_2(ppy)_2(\mu\text{-}Cl)_2$ with 5-[2-(4-substituent-phenyl)ethynyl]-8-quinolinol ligands in the presence of $Na_2CO_3$ (Scheme 1). All complexes were fully characterized by elemental analyses, HRMS, $^1H(^{13}C)$ NMR and IR spectroscopy. The crystal structure of **1** was determined by X-ray crystallography. Interestingly, when **4** was recrystallized from different organic solvents, three kinds of pseudopolymorphs with different color, luminescence and stacking structures, including five orange solvated samples {**4**·½(Toluene), **4**·$CH_3CH_2OH$, **4**·½($Et_2O$), **4**·½($CH_3OH$), and **4**·½(Hexane)}, a red solvent-free sample **4R**, and a dark-brown sample **4**·½($CCl_4$), were isolated (Figs. S1–S5). This phenomenon indicates that complex **4** may have luminescence switching property. Five orange solvated samples have almost the same PXRD pattern, revealing that they have the same and very stable molecular framework constructed by Pt(II) moieties (Fig. S1). In contrast, only red solvent-free species could be obtained when **1**–**3** were recrystallized from these solvents (Figs. S6–S9).

Fig. 1a shows the molecular structure of complex **1** and its selected bond lengths and angles are given in Table S2 as the supporting information. The Pt center of **1** is coordinated by $C_1N_2O$ atoms and adopted a square-planar geometry with four *cis*-angles around the platinum center in the range 80.38–106.0° (Table S2). Two coordinated N atoms from ppy and 8-quinolinol ligands are in the opposite position. The molecule of **1** displays good planarity with the dihedral angle between ppy and 8-quinolinol ligands being 9.15°. Along *a* axis, adjacent molecules are paralleled in the same direction and connected with each other through π-π stacking interactions to form the one-dimensional scalene cylinder structure (Fig. 1b and Table S3). Because of the large slip between adjacent molecules, the shortest Pt···Pt distance is 6.600 Å, indicating no intermolecular Pt-Pt contact exists in the stacking structure (Table S2). The molecules in neighboring scalene cylinder structures along *b* axis are arranged in the opposite directions and connected by strong hydrogen bonds (Fig. 1c and Table S3). The dihedral angles between molecules in adjacent scalene cylinder structures are 26.31°. The molecules in adjacent scalene cylinder structures along *c* axis exhibit a head-to-head structure with larger dihedral angles (64.35°) (Fig. S10). This kind of arrangement allows the compact stacking of molecules through strong C-H···π hydrogen bonding network (Fig. S1 and Table S3). Complexes **2** and **3** may also have the compact stacking structure, whereas **4** most likely stacks in a relatively loose stacking structure considering the steric hindrance of their substituents.

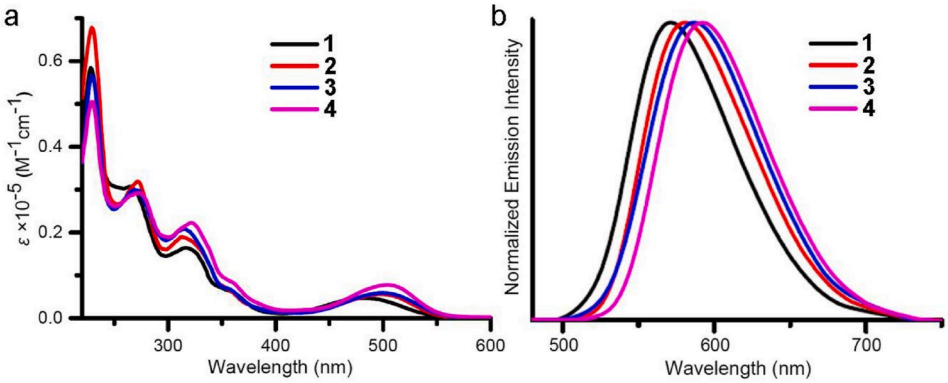


**Fig. 2.** The UV–Vis absorption (a) and emission spectra (b) of complex **1–4** in $CH_2Cl_2$ solution: **1**, 0.017 mM; **2**, 0.024 mM; **3**, 0.021 mM; **4**, 0.018 mM.

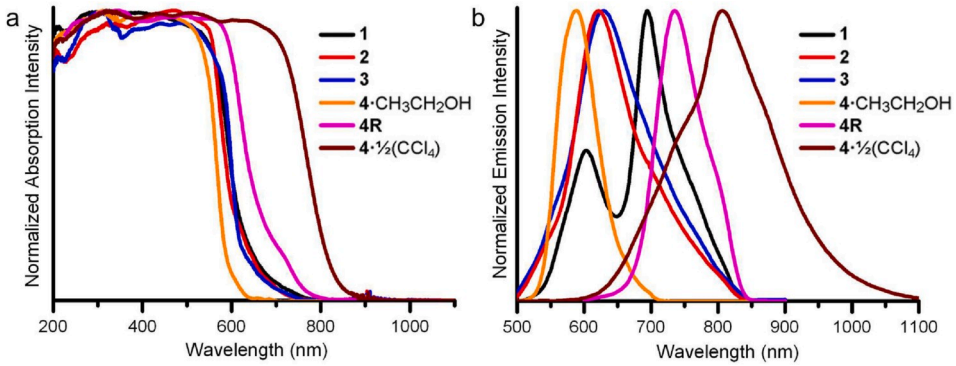


**Fig. 3.** The UV–Vis absorption (a) and emission spectra (b) of complexes **1–3**, **4**·$CH_3CH_2OH$, **4R** and **4**·½($CCl_4$) in solid state.

**Table 1**
Luminescence data of **1**–**4** in different states at ambient temperature.

| Sample | medium | $\lambda_{em}$ (nm) | $\tau_{em}$ (μs) | $\Phi_{em}$ (%) |
|---|---|---|---|---|
| **1** | $CH_2Cl_2$ solution | 572 | 4.65 | 0.19[a] |
| | solid state | 600, 693 | 4.97, 0.074 | 0.24 |
| **2** | $CH_2Cl_2$ solution | 582 | 2.71 | 0.15[a] |
| | solid state | 621 | 2.80 | 0.05 |
| **3** | $CH_2Cl_2$ solution | 586 | 6.13 | 0.16[a] |
| | solid state | 627 | 2.94 | 0.04 |
| **4** | $CH_2Cl_2$ solution | 592 | 2.42 | 0.20[a] |
| **4**·$CH_3CH_2OH$ | solid state | 586 | 3.60 | 0.29 |
| **4R** | solid state | 735 | 1.87 | 0.35 |
| **4**·½($CCl_4$) | solid state | 808 | 0.84 | <0.01 |
| **4O** | heated | 586 | 3.45 | 0.27 |
| **4G** | ground | 742 | 1.56 | 0.24 |

[a] The quantum yield was estimated relative to $[Ru(bpy)_3](PF_6)_2$ in $CH_3CN$ as the standard ($\Phi_{em}$ = 6.2%).

### 3.2. Photophysical properties

The absorption properties of all complexes **1–4** were measured in dichloromethane at room temperature (Fig. 2a). The spectra all reveal strong absorption bands between 225 and 360 nm mainly corresponding to intraligand $^1$IL (ppy and 8-quinolinol ligands) charge transitions. The low-energy absorption bands centered at 480 nm for **1**, 498 nm for **2**, 500 nm for **3**, and 503 nm for **4** can be assigned to π(5-substituted-8-quinolinol) → π*(ppy) ligand-to-ligand charge transfer ($^1$LLCT) and dπ (Pt) → π*(ppy) metal-to-ligand charge transfer ($^1$MLCT) transitions according to the literatures [56,59,64]. All complexes display an orange-red luminescence in dilute $CH_2Cl_2$ solution with maximum emission band centered at 572 nm for **1**, 582 nm for **2**, 586 nm for **3**, and 592 nm for **4**, resulting from the admixture of $^3$LLCT and $^3$MLCT triplet states. The red-shift of low-energy absorption and emission bands from **1** to **4** are result from the electronic effect of substituents on 8-quinolinol ligand.

In solid state, the red forms of **1-3** exhibit similar UV–Vis absorption spectra with low-energy absorption bands at about 450–555 nm (Fig. 3a). The low-energy bands of orange sample **4**·$CH_3CH_2OH$ display a slight blue-shift compared with those of **1-3** and occurred at 440–540 nm (Fig. 3a). All of them can be attributed to $^1$LLCT and $^1$MLCT transitions. Their difference in low-energy absorption bands are mostly likely due to the existence of intermolecular aromatic π-π stacking interactions in red samples. Compared to those of **1-3** and **4**·$CH_3CH_2OH$, the low-energy absorption of red **4R** in the range of 580–800 nm displays a noticeable red shift most likely due to the $^1$MMLCT (metal-metal to ligand charge transfer) transition based on existence of Pt-Pt interactions in the stacking structure (Fig. 3a). In comparison, the dark-brown **4**·½($CCl_4$) displays a distinct new low-energy absorption band at 701 nm extending to 900 nm, indicating that it originates from the different attribution (Fig. 3a). As this new absorption band is one of the

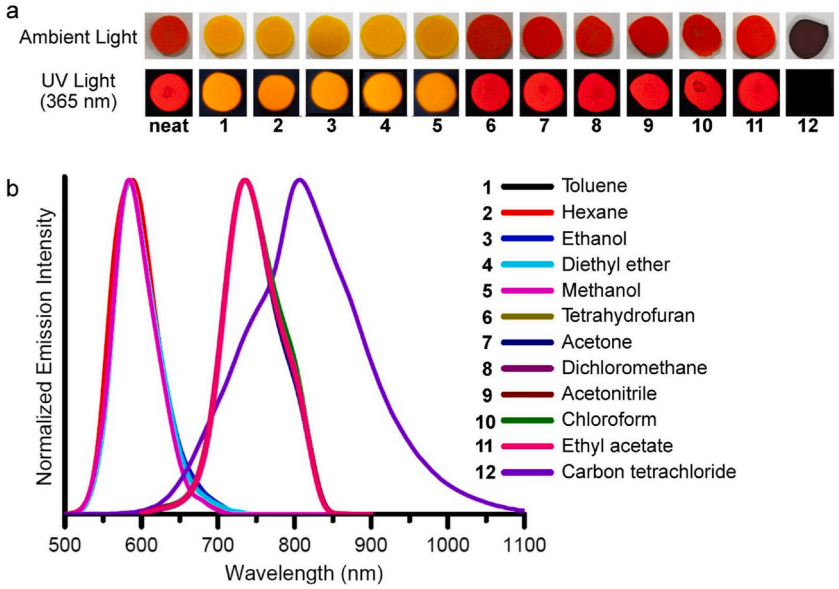


**Fig. 4.** Vapoluminescence of complex **4**. (a) Photographic images under ambient light and UV light irradiation ($\lambda_{ex}$ = 365 nm) and (b) emission spectra of **4R** after exposure to different VOC vapors.

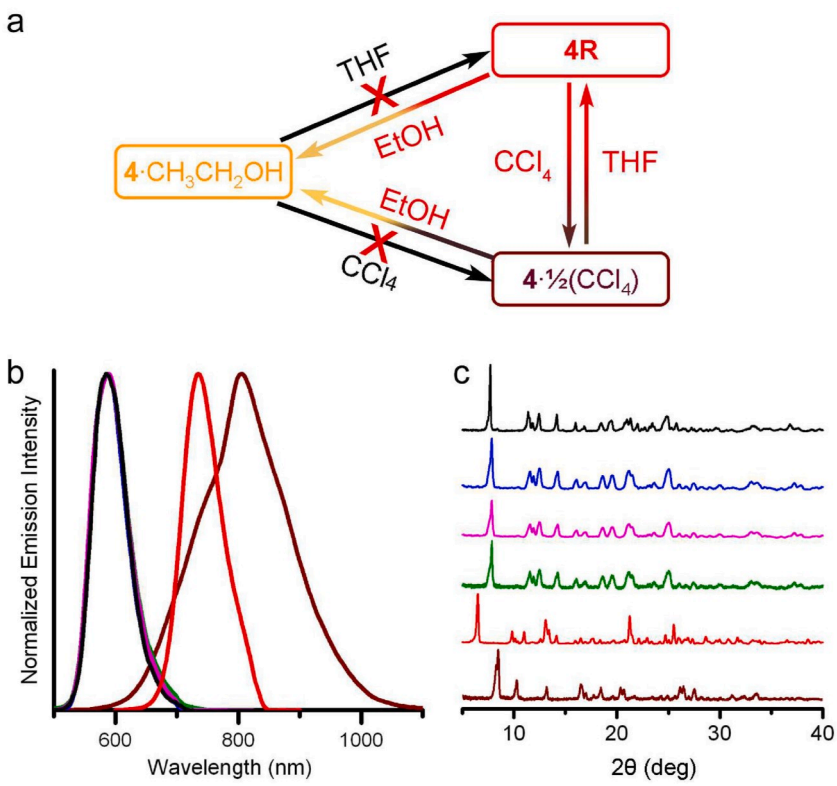


**Fig. 5.** The vapor-triggered irreversible structural conversion of **4**. (a) The conversion routes of **4**·$CH_3CH_2OH$, **4R** and **4**·½($CCl_4$) upon exposure to corresponding VOC vapors. (b) The emission spectra and (c) PXRD patterns of **4**·$CH_3CH_2OH$ after absorbing THF (black) and $CCl_4$ (blue) vapor; **4R** after absorbing ethanol (magenta) and $CCl_4$ (wine) vapor; and **4**·½($CCl_4$) after absorbing ethanol (olive) and THF (red) vapor. (For interpretation of the references to color in this figure legend, the reader is referred to the Web version of this article.)

characteristics of Pt(II) complex with 1-D "platinum wire" stacking structure, there is no doubt it derives from the $^1$MMLCT transition [20,36].

Under irradiation at 460 nm, **1** shows a distinct emission profile with two components peaked at 600 and 693 nm, respectively (Fig. 3b and Table 1). The high-energy emission band at 600 nm has a little red-shift compared with its emission band in solution, revealing the same emission origin of them. As no Pt-Pt interaction exists in **1**, the lower-energy transition at 693 nm can not be $^3$MMLCT, so we suggest that it is the exciplex emission generated by intermolecular aromatic π-π interactions according to the literatures [58,73–76]. The red solid sample **2** and **3** exhibit the similar red luminescence with a broad emission band peaked at 621 nm and 627 nm, respectively (Fig. 3b and Table 1). Both of them arise from the $^3$LLCT and $^3$MLCT transitions. The yellow **4**·$CH_3CH_2OH$ displays the yellow-orange luminescence peaked at 586 nm which is similar with its emission in $CH_2Cl_2$ solution (Fig. 3b and Table 1). Whereas, **4R** emits a red luminescence with broad emission band centered at 735 nm (Fig. 3b and Table 1). The significant large red-shift of emission compared with that of **4**·$CH_3CH_2OH$ demonstrates that the emission of **4R** most likely originates from $^3$MMLCT transition. More interestingly, under visible light (460 nm) irradiation, dark-brown **4**·½($CCl_4$) emits an unusual NIR luminescence peaked at 808 nm (Fig. 3b and Table 1) possibly mainly because of the formation of 1-D "platinum wire" stacking structure with strong Pt-Pt interactions and thus further reduced energy level of $^3$MMLCT excited state. To the best of our knowledge, it is the first Pt(II) complex bearing 8-quinolinol derivatives that exhibits NIR luminescence beyond 800 nm in the solid state.

### 3.3. Vapoluminescence

The vapoluminescent properties of **1-4** were explored. Upon exposure to different VOC vapors, there is no change in the color and luminescence of complexes **1–3**, indicating they haven't vapoluminescent property (Figs. S11–S13). The reason is most likely due to their compact and stable stacking structures that prevents the structural conversion of them once exposure to VOC vapor.

In contrast, **4** exhibits unusual irreversible vapoluminescent property. As shown in Fig. 4, once exposure to toluene, hexane, ethanol, diethyl ether, or methanol vapors, both the color and luminescence of red **4R** were changed from red to orange accompanied with the blue shift of emission spectra from 735 nm to *ca.* 586 nm. Meanwhile, the sample exposure to $CCl_4$ vapor changed to the dark-brown color and the original red luminescence was quenched. The luminescence spectrum, TGA and PXRD measurements confirmed that this dark-brown sample is **4**·½($CCl_4$) (Figs. S14 and S15). In contrast, there is no any change in color and luminescence of the sample exposed to THF, acetone, $CH_2Cl_2$, $CH_3CN$, $CHCl_3$, or ethyl acetate vapors (Fig. 4). These results are in good agreement with the fact that **4** recrystallized from different solvents. The interconversions between orange sample (**4**·$CH_3CH_2OH$ is selected as the representative), **4R** and **4**·½($CCl_4$) were also studied (Fig. 5). We have known that **4R** can be converted to **4**·$CH_3CH_2OH$ or **4**·½($CCl_4$) once absorbing ethanol or $CCl_4$ vapors, respectively. When **4**·½($CCl_4$) was exposed to ethanol or THF vapor, **4**·$CH_3CH_2OH$ and **4R** can also converted as confirmed by luminescence spectra and PXRD measurements (Fig. 5b–c). To our surprise, **4**·$CH_3CH_2OH$ can not be changed to **4R** or **4**·½($CCl_4$) by vapor absorption. The results indicate that the vapoluminescent property of **4** is not fully reversible. As vapoluminescence of square-planar Pt(II) complexes are usually caused by the structural conversion and consequent changes in weak intermolecular interactions, most vapoluminescent behaviours of Pt(II) complexes are reversible, and only a few examples about irreversible vapoluminescent behaviours have been reported up until now [36,68,77–80]. The results demonstrate that the molecular framework of **4**·$CH_3CH_2OH$ may have a better stability than that of **4R** and **4**·½($CCl_4$). Thus, **4R** and **4**·½($CCl_4$) can be changed to other forms triggered by vapor absorption, while **4**·$CH_3CH_2OH$ could not. Furthermore, the vapoluminescence behaviour of **4** can be attributed to the changes of the lowest-excited states between LLCT/MLCT and MMLCT transitions caused by structural conversions triggered by vapor absorption. Meanwhile, the experimental results

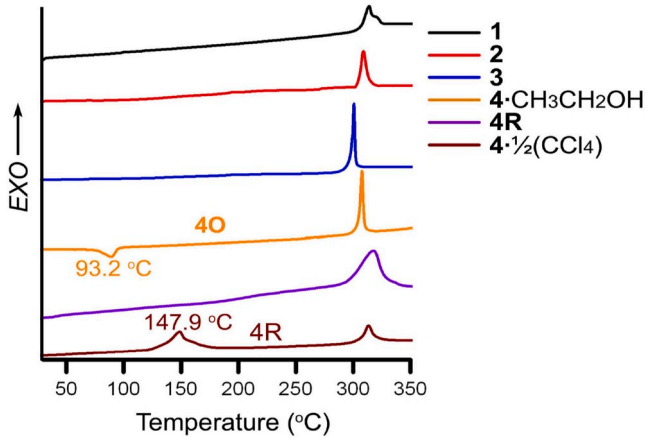


**Fig. 6.** DSC curves of complexes **1–4** under the $N_2$ atmosphere at a heating rate of 5 °C/min.

suggest that Pt(II) complex with stable and compact stacking structure may be not conductive to generation of vapoluminescent property.

### 3.4. Thermochromic luminescence

We also explored the responses of complexes **1–4** to heat. As shown in Fig. 6, complexes **1–3** and **4R** haven't any change before decomposition during the heating process, revealing they don't have thermochromic luminescence property.

Upon heating to 300 °C, **4**·$CH_3CH_2OH$ experience a phase transition at 93.2 °C, corresponding to the transformation from **4**·$CH_3CH_2OH$ to **4O** caused by the loss of $CH_3CH_2OH$ solvent (Figs. 6 and 7 and Fig. S16). The new polymorphs **4O** has the same color, luminescence and PXRD pattern with those of **4**·$CH_3CH_2OH$ and can be easily restored to original **4**·$CH_3CH_2OH$ by absorbing $CH_3CH_2OH$ vapor (Fig. 7). Although solvated $CH_3CH_2OH$ was lost during the heating, **4**·$CH_3CH_2OH$ has not thermochromic luminescence because **4O** has the same stabled molecular framework with that of **4**·$CH_3CH_2OH$.

In contrast, once **4**·½($CCl_4$) is heated at 155 °C, the color of the sample changes to red (Fig. 7). This red sample does not contain any solvent molecules and emits a red luminescence peaked at 735 nm (Fig. 7b and Table 1). The PXRD measurement confirms that this red sample is **4R** (Fig. 7c). It's well known that 1-D "platinum wire" stacking structures have weak intermolecular interactions and large spaces between neighboring columns, they are usually broken and transformed to dimeric with Pt-Pt interaction under external stimuli. The thermochromic luminescence of **4**·½($CCl_4$) is fully reversible as **4R** can easily be converted to **4**·½($CCl_4$) upon exposure to $CCl_4$ vapor. So, the mechanism of thermochromic luminescence of **4**·½($CCl_4$) is the conversion of the 1-D "platinum wire" stacking structure to dimeric structure with intermolecular Pt-Pt interaction upon heating and the resultant changes of the lowest-excited state energy levels.

### 3.5. Mechanoluminescence

Upon mechanical grinding, the color and luminescence of complexes **1–3** have no visibly discernible change although PXRD measurement indicate that they have changed from crystalline state to amorphous phase (Figs. S17–S20). The result demonstrates that grinding force could not change their energy level of lowest excited states. Therefore, complexes **1–3** have not mechanoluminescent property and the most likely reason is their compact stacking structures.

In contrast, the color and luminescence of **4**·$CH_3CH_2OH$ and **4**·½($CCl_4$) changed to red after ground, whereas those of **4R** have no visibly discernible change, revealing both **4**·$CH_3CH_2OH$ and **4**·½($CCl_4$) have the mechanoluminescence behaviour (Fig. 8, Fig. 9 and Fig. S21). The ground samples of them are all in an amorphous phase and display the same luminescence spectra with maximum emission wavelength peaked at 742 nm (Fig. 8 and Table 1), indicating they are the same product (namely **4G**). The corresponding luminescence response shifts of them to the mechanical grinding are *ca.* 156 nm for **4**·$CH_3CH_2OH$, 7 nm for **4R**, and −66 nm for **4**·½($CCl_4$). The large red-shift of **4**·$CH_3CH_2OH$ indicates the change of its excited state from original $^3$LLCT/$^3$MLCT to the $^3$MMLCT transitions. Interestingly, the response of

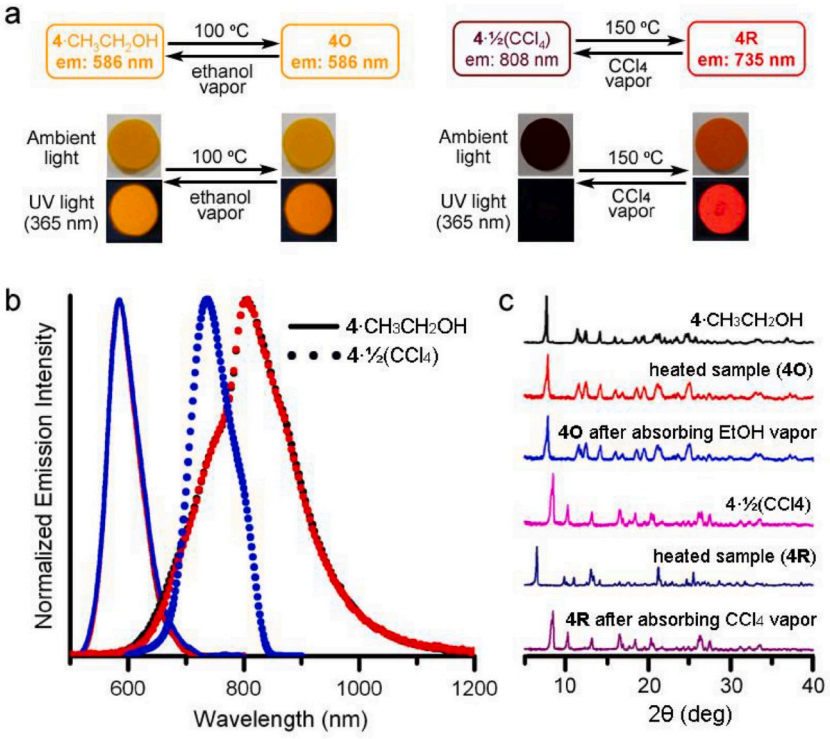


**Fig. 7.** Thermochromic luminescence of **4**. (a) The conversion routes and photographic images of **4**·$CH_3CH_2OH$ and **4**·½($CCl_4$) under ambient light and UV light (365 nm) irradiation during a reversible process of heating and vapor absorbing. (b) The luminescence spectra of **4**·$CH_3CH_2OH$ and **4**·½($CCl_4$) in different states: crystalline state (black color), heated state (red color) and the restored state by exposure heated samples to $CH_3CH_2OH$ or $CCl_4$ vapor (blue color). (c) PXRD patterns of **4**·$CH_3CH_2OH$ and **4**·½($CCl_4$) during a heating-vapor absorbing process. (For interpretation of the references to color in this figure legend, the reader is referred to the Web version of this article.)

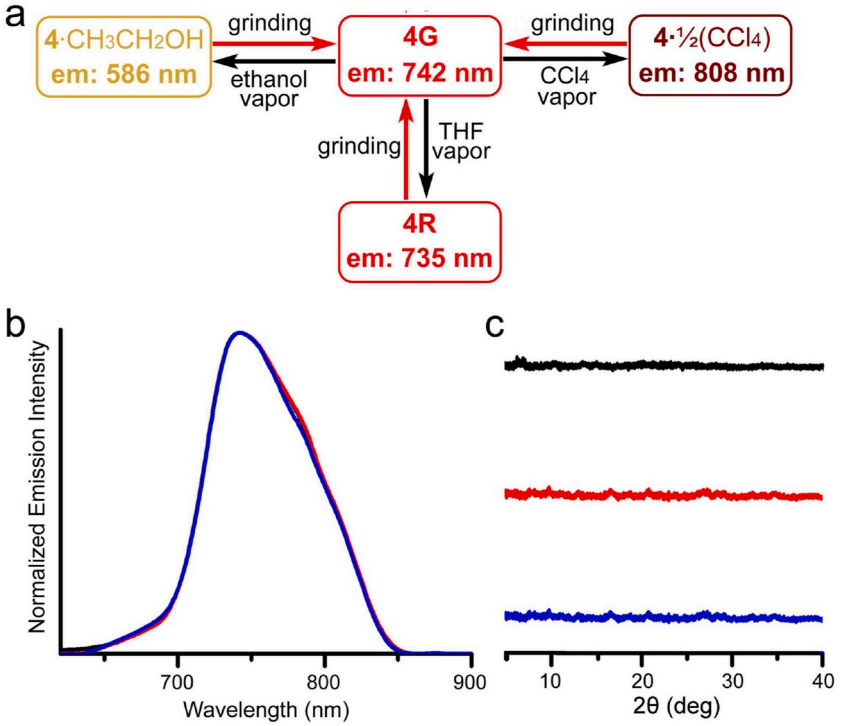


**Fig. 8.** Mechanoluminescence of **4**. (a) The reversible conversion routes of **4**·$CH_3CH_2OH$, **4R**, and **4**·½($CCl_4$) in response to mechanical grinding and restored by vapor absorbing. (b) The luminescence spectra and (c) PXRD patterns of **4**·$CH_3CH_2OH$ (black line), **4R** (red line), and **4**·½($CCl_4$) (blue line) after ground. (For interpretation of the references to color in this figure legend, the reader is referred to the Web version of this article.)

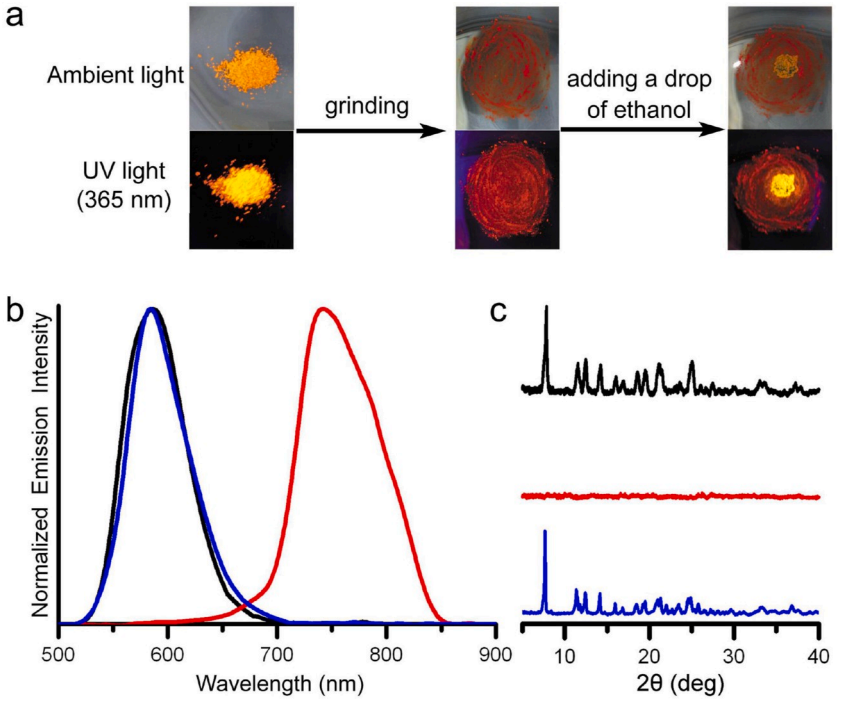


**Fig. 9.** The reversible mechanoluminescence of **4**·$CH_3CH_2OH$. (a) Photographic images of samples under ambient light and UV light (365 nm) irradiation during the reversible process. (b) Emission spectra and (c) PXRD patterns of unground sample (black line), ground sample (red line), and ground sample with a drop of ethanol added (blue line). (For interpretation of the references to color in this figure legend, the reader is referred to the Web version of this article.)

**4R** to mechanical grinding only has 7 nm. The results show that the luminescence of **4R** and **4G** originates from the same excited state, and the existence of Pt-Pt contact in **4G** is also confirmed. For **4**·½($CCl_4$), mechanical grinding lead to a 66 nm blue shift in the emission spectrum. The blue shift in emission is caused by the breaking of 1-D "platinum wire" structure into the amorphous phase (existence of Pt-Pt contact) and resultant increasing of energy gap between HOMO and LUMO.

Once either exposed to $CH_3CH_2OH$ or $CCl_4$ vapor or a drop of

$CH_3CH_2OH$ or $CCl_4$ was added, the color, luminescence and PXRD patterns of **4G** could be converted back to the original crystalline states of **4**·$CH_3CH_2OH$ or **4**·½($CCl_4$), respectively (Fig. 9 and Fig. S21). In fact, **4G** could also be restored to **4R** after exposure to THF vapor (Fig. S22). Therefore, the mechanoluminescence property of **4**·$CH_3CH_2OH$ and **4**·½($CCl_4$) are fully reversible. The emission wavelength and intensity of both **4**·$CH_3CH_2OH$ and its ground sample have no evident changes even after 20-cycles of grinding/solvent-adding process (Fig. S23). It is well known that the mechanical grinding can result the desorption of the solvent molecule from a solvated complex which may also lead to the changes in color and luminescence. However, the mechanoluminescence of **4**·$CH_3CH_2OH$ and **4**·½($CCl_4$) are not due to the desorption of the solvent molecules because their ground sample are quite different with their heated samples.

## 4. Conclusions

In summary, four square-planar cycloplatinated(II) complexes based on 5-substituted-8-quinolinol derivatives and 2-phenylpyridine ligand have been designed and synthesized. Complexes **1**–**3** were isolated as red desolvated samples. Whereas, three main types of **4** were obtained, namely, orange **4**·$CH_3CH_2OH$, red **4R** and dark-brown **4**·½($CCl_4$). Among them the dark-brown **4**·½($CCl_4$) exhibits a NIR luminescence peaked at 808 nm, which is the longest luminescent wavelength of reported Pt(II) complex based on 8-quinolinol derivatives to the best of our knowledge. Complexes **1**–**3** show no detectable response to VOC vapors, heating, or mechanical grinding, indicating they have not vapoluminescent, thermochromic luminescent and mechanoluminescent properties. In contrast, **4** exhibits tri-stimuli-responsive luminescence switching property caused by structural conversion and resultant changes of the lowest-energy excited states. Upon exposure to VOC vapors, **4** exhibited unusual irreversible vapoluminescent property which is mainly due to the compact stacking structure of **4**·$CH_3CH_2OH$. Furthermore, both orange **4**·$CH_3CH_2OH$ and dark-brown **4**·½($CCl_4$) also displayed reversible responses to heating and mechanical grinding. Considering that the only difference of **1-4** is their substituents, the different response of **4** to external stimuli compared with that of **1-3** is mainly due to the large steric hindrance of tert-butyl group which results the loose stacking structure and possibility of structural conversion.

## Notes

The authors declare no competing financial interest.

## Declaration of competing interest

The authors declare that they have no known competing financial interests or personal relationships that could have appeared to influence the work reported in this paper.

## CRediT authorship contribution statement

**Jun Ni:** Project administration, Writing - original draft, Formal analysis, Funding acquisition. **Gao Liu:** Data curation, Investigation, Formal analysis. **Mengmeng Su:** Formal analysis. **Wei Zheng:** Formal analysis. **Jianjun Zhang:** Formal analysis, Funding acquisition.

## Acknowledgements

This work is financially supported by the National Natural Science Foundation of China (21471024, 21871038).

## Appendix A. Supplementary data

Supplementary data to this article can be found online at https://doi.org/10.1016/j.dyepig.2020.108451.

## References

[1] Fleetham T, Li GJ, Li J. Phosphorescent Pt(II) and Pd(II) complexes for efficient, high-color-quality, and stable OLEDs. Adv Mater 2017;29:1601861.
[2] Tseng CH, Fox MA, Liao JL, Ku CH, Sie ZT, Chang CH, Wang JY, Chen ZN, Lee GH, Chi Y. Luminescent Pt(II) complexes featuring imidazolylidene-pyridylidene and dianionic bipyrazolate: from fundamentals to OLED fabrications. J Mater Chem C 2017;5:1420–35.
[3] Wang X, Wang SN. Phosphorescent Pt(II) emitters for OLEDs: from triarylboron-functionalized bidentate complexes to compounds with macrocyclic chelating ligands. Chem Rec 2019;19:1693–709.
[4] Strassner T. Phosphorescent platinum(II) complexes with C^C* cyclometalated NHC ligands. Accounts Chem Res 2016;49:2680–9.
[5] Li GJ, Zhao XD, Fleetham T, Chen QD, Zhan F, Zheng JB, Yang YF, Lou WW, Yang YN, Fang K, Shao ZZ, Zhang QS, She YB. Tetradentate platinum(II) complexes for highly efficient phosphorescent emitters and sky blue OLEDs. Chem Mater 2020;32:537–48.
[6] Samiee S, Hossienpour P. A comparative theoretical study on the optoelectronic and nonlinear optical properties of [Pt(bpy)(qdt)] derivatives with electron-donating and -withdrawing anchors. New J Chem 2019;43:12865–73.
[7] Zhong FF, Zhao JZ. An platinum(II) bis(acetylide) complex with naphthalimide and pyrene ligands: synthesis, photophysical properties, and application in triplet-triplet annihilation upconversion. Eur J Inorg Chem 2017:5196–204.
[8] Wang PL, Koo YH, Kim W, Yang WB, Cui XN, Ji W, Zhao JZ, Kim D. Broadband visible light harvesting N^N Pt(II) bisacetylide complex with bodipy and naphthalene diimide ligands: förster resonance energy transfer and intersystem crossing. J Phys Chem C 2017;121:11117–28.
[9] Cai WL, Zhao AC, Ren K, He RX, Li M, Shen W. Understanding the mechanisms of white light emission of a tetradentate Pt complex in various surrounding environments. J Phys Chem C 2019;123:17968–75.
[10] Yan ZP, Luo XF, Liu WQ, Wu ZG, Liang X, Liao K, Wang Y, Zheng YX, Zhou L, Zuo JL, Pan Y, Zhang HJ. Configurationally stable platinahelicene enantiomers for efficient circularly polarized phosphorescent organic light-emitting diodes. Chem Eur J 2019;25:5672–6.
[11] Bachmann M, Suter D, Blacque O, Venkatesan K. Tunable and efficient white light phosphorescent emission based on single component N-heterocyclic carbene platinum(II) complexes. Inorg Chem 2016;55:4733–45.
[12] Chi Y, Chou PT. Transition-metal phosphors with cyclometalating ligands: fundamentals and applications. Chem Soc Rev 2010;39:638–55.
[13] Li K, Tong GSM, Wang QY, Cheng G, Tong WY, Ang WH, Kwong WL, Che CM. Highly phosphorescent platinum(II) emitters: photophysics, materials and biological applications. Chem Sci 2016;7:1653–73.
[14] Zhang KY, Yu Q, Wei HJ, Liu SJ, Zhao Q, Huang W. Long-lived emissive probes for time-resolved photoluminescence bioimaging and biosensing. Chem Rev 2018;118:1770–839.
[15] Mauro M, Aliprandi A, Septiadi D, Kehr NS, De Cola L. When self-assembly meets biology: luminescent platinum complexes for imaging applications. Chem Soc Rev 2014;43:4144–66.
[16] Law ASY, Lee LCC, Yeung MCL, Lo KKW, Yam VWW. Amyloid Protein-induced supramolecular self-assembly of water-soluble platinum(II) complexes: a luminescence assay for amyloid fibrillation detection and inhibitor screening. J Am Chem Soc 2019;141:18570–7.
[17] Wong KMC, Yam VWW. Self-assembly of luminescent alkynylplatinum(II) terpyridyl complexes: modulation of photophysical properties through aggregation behavior. Acc Chem Res 2011;44:424–34.
[18] Yam VWW, Au VKM, Leung SYL. Light-emitting self-assembled materials based on $d^8$ and $d^{10}$ transition metal complexes. Chem Rev 2015;115:7589–728.
[19] Law ASY, Yeung MCL, Yam VWW. Arginine-rich peptide-induced supramolecular self-assembly of water-soluble anionic alkynylplatinum(II) complexes: a continuous and label-free luminescence assay for trypsin and inhibitor screening. ACS Appl Mater Interfaces 2017;9:41143–50.
[20] Kang JJ, Zhang XX, Zhou HJ, Gai XQ, Jia T, Xu L, Zhang JJ, Li YQ, Ni J. 1-D "platinum wire" stacking structure built of platinum(II) diimine bis(σ-acetylide) units with luminescence in the NIR region. Inorg Chem 2016;55:10208–17.
[21] Kobayashi A, Kato M. Vapochromic platinum(II) complexes: crystal engineering toward intelligent sensing devices. Eur J Inorg Chem 2014:4469–83.
[22] Zhang X, Wang JY, Ni J, Zhang LY, Chen ZN. Vapochromic and mechanochromic phosphorescence materials based on a platinum(II) complex with 4-trifluoromethylphenylacetylide. Inorg Chem 2012;51:5569–79.
[23] Ni J, Zhang X, Wu YH, Zhang LY, Chen ZN. Vapor- and mechanical-grinding-triggered color and luminescence switches for bis(σ-fluorophenylacetylide) platinum(II) complexes. Chem Eur J 2011;17:1171–83.
[24] Yam WVV, Hu YC, Chan KHY, Chung CYS. Reversible pH- and solvent-responsive micelle-mediated self-assembly of platinum(II) terpyridyl-based metallo-supramolecular diblock copolymers. Chem Commun 2009:6216–8.
[25] Krikorian M, Liu S, Swager TM. Columnar liquid crystallinity and mechanochromism in cationic platinum(II) complexes. J Am Chem Soc 2014;136:2952–5.
[26] Krikorian M, Voll CCA, Yoon M, Venkatesan K, Kouwer PH, Swager TM. Smectic A mesophases from luminescent sandic platinum(II) mesogens. Liq Cryst 2016;43:1709–13.
[27] Venkatesan K, Kouwer PHJ, Yagi S, Müller P, Swager YM. Columnar mesophases from half-discoid platinum cyclometalated metallomesogens. J Mater Chem 2008;18:400–7.
[28] Cuerva C, Campo JA, Ovejero P, Torres MR, Oliveira E, Santos SM, Lodeiro C, Cano M. Columnar discotic Pt(ii) metallomesogens as luminescence

multifunctional materials with chemo and thermosensor abilities. J Mater Chem C 2014;2:9167–81.
[29] Thomas SW, Venkatesan K, Müller P, Swager TM. Dark-field oxidative addition-based chemosensing: new bis-cyclometalated Pt(II) complexes and phosphorescent detection of cyanogen halides. J Am Chem Soc 2006;128:16641–8.
[30] Cuerva C, Campo JA, Cano M, Lodeiro C. Multi-stimuli-responsive properties of aggregation-enhanced emission-active unsymmetrical $Pt^{II}$ metallomesogens through self-assembly. Chem Eur J 2019;25:12046–51.
[31] Cuerva C, Campo JA, Cano M, Lodeiro C. Platinum(II) metallornesogens: new external-stimuli-responsive photoluminescence materials. Chem Eur J 2016;22:10168–78.
[32] Cheng S, Liu SJ, Zhou LX, Xu WJ, Zhao Q, Huang W. Phosphorescent chemosensors for metal cations based on heavy-metal complexes. Prog Chem 2011;23:679–86.
[33] Wong KMC, Yam VWW. Luminescence platinum(II) terpyridyl complexes - from fundamental studies to sensory functions. Coord Chem Rev 2007;251:2477–88.
[34] Kato M, Omura A, Toshikawa A, Kishi S, Sugimoto Y. Vapor-induced luminescence switching in crystals of the syn isomer of a dinuclear (bipyridine)platinum(II) complex bridged with pyridine-2-thiolate ions. Angew Chem Int Ed 2002;41:3183–98.
[35] Qiu DF, Li MM, Zhao Q, Wang HW, Yang CX. Cyclometalated platinum(II) terpyridylacetylide with a bis(arylamine) donor as a proton-triggered luminescence chemosensor for $Zn^{2+}$. Inorg Chem 2015;54:7774–82.
[36] Kang JJ, Ni J, Su MM, Li YQ, Zhang JJ, Zhou HJ, Chen ZN. Facile and equipment-free data encryption and decryption by self-encrypting Pt(II) complex. ACS Appl Mater Interfaces 2019;11:13350–8.
[37] Zhang XQ, Chi ZG, Zhang Y, Liu SW, Xu JR. Recent advances in mechanochromic luminescent metal complexes. J Mater Chem C 2013;1:3376–90.
[38] Cuerva C, Campo JA, Cano M, Arredondo B, Romero B, Oton E, Oton JM. Bis(pyridylpyrazolate)platinum(II): a mechanochromic complex useful as a dopant for colour-tunable polymer OLEDs. New J Chem 2015;39:8467–73.
[39] Haque A, Xu LL, Al-Balushi RA, Al-Suti MK, IIMi R, Guo ZL, Khan MS, Wong WY, Raithby PR. Cyclometallated tridentate platinum(II) arylacetylide complexes: old wine in new bottles. Chem Soc Rev 2019;48:5547–63.
[40] Sicilia V, Arnal L, Chueca AJ, Fuertes S, Babaei A, Munõz AMI, Sessolo M, Bolink HJ. Highly photoluminescent blue ionic platinum-based emitters. Inorg Chem 2020;59:1145–52.
[41] Cheng G, Wan QY, Ang WH, Kwong CL, To WP, Chow PK, Kwok CC, Che CM. High-performance deep-red/near-infrared OLEDs with tetradentate [Pt(O^N^C^N)] emitters. Adv Optical Mater 2019;7:1801452.
[42] Zhang YM, Chen Z, Wang X, He JJ, Wu JT, Liu HY, Song J, Qu JL, Chan WTK, Wong WY. Achieving NIR emission for donor–acceptor type platinum(II) complexes by adjusting coordination position with isomeric ligands. Inorg Chem 2018;57:14208–17.
[43] Wilde S, Ma DX, Koch T, Bakker A, Gonzalez-Abradelo D, Stegemann L, Daniliuc CG, Fuchs H, Gao HY, Doltsinis NL, Duan L, Strassert CA. Toward tunable electroluminescent devices by correlating function and submolecular structure in 3D crystals, 2D-confined monolayers, and dimers. ACS Appl Mater Interfaces 2018;10:22460–73.
[44] Zhong JJ, Yang C, Chang XY, Zou C, Lu W, Che CM. Platinum(ii) photo-catalysis for highly selective difluoroalkylation reactions. Chem Commun 2017;53:8948–51.
[45] Choi WJ, Choi SK, Ohkubo K, Fukuzumi S, Cho EJ, You YM. Mechanisms and applications of cyclometalated Pt(II) complexes in photoredox catalytic trifluoromethylation. Chem Sci 2015;6:1454–64.
[46] Shelar DP, Li TT, Chen Y, Fu WF. Platinum(II) schiff base complexes as photocatalysts for visible-light-induced cross- dehydrogenative coupling reactions. ChemPlusChem 2015;80:1541–6.
[47] González-Muñoz D, Casado-Sánchez A, del Hierro I, Gómez-Ruiz S, Cabrera S, Alemán J. Size-selective mesoporous silica-based Pt(II) complex as efficient and reusable photocatalytic material. J Catal 2019;373:374–83.
[48] Vezzu DAK, Ravindranathan D, Garner AW, Bartolotti L, Smith ME, Boyle PD, Hou SQ. Highly luminescent tridentate N^C*N platinum(II) complexes featured in fused five-six-membered metallacycle and diminishing concentration quenching. Inorg Chem 2011;50:8261–73.
[49] Casado-Sánchez A, Gómez-Ballesteros R, Tato F, Soriano FJ, Pascual-Coca G, Cabrera S, Alemán J. Pt(II) coordination complexes as visible light photocatalysts for the oxidation of sulfides using batch and flow processes. Chem Commun 2016;52:9137–40.
[50] Zhou GJ, Wong WY, Yang XL. New design tactics in OLEDs using functionalized 2-phenylpyridine-type cyclometalates of iridium(III) and platinum(II). Chem Asian J 2011;6:1706–27.
[51] Zhou GJ, Wang Q, Wong WY, Ma DG, Wang LX, Lin ZY. A versatile color tuning strategy for iridium(III) and platinum(II) electrophosphors by shifting the charge-transfer states with an electron-deficient core. J Mater Chem 2009;19:1872–83.
[52] Ebina M, Kobayashi A, Ogawa T, Yoshida M, Kato M. Impact of a carboxyl group on a cyclometalated ligand: hydrogen-bond- and coordination-driven self-assembly of a luminescent platinum(II) complex. Inorg Chem 2015;54:8878–80.
[53] Liang AH, Li YH, Zhu WG, Wang YF, Huang F, Wu HB, Cao Y. Novel cyclometalated platinum(II) complex containing carrier-transporting groups: synthesis, luminescence and application in single dopant white PLEDs. Dyes Pigments 2013;96:732–7.
[54] Yu JT, He KQ, Li YH, Tan H, Zhu MX, Wang YF, Liu Y, Zhu WG, Wu HB. A novel near-infrared-emitting cyclometalated platinum(II) complex with donor-acceptor-acceptor chromophores. Dyes Pigments 2014;107:146–52.
[55] Stacey OJ, Platts JA, Coles SJ, Horton PN, Pope SJA. Phosphorescent, cyclometalated cinchophen-derived platinum complexes: syntheses, structures, and electronic properties. Inorg Chem 2015;54:6528–36.
[56] Yang CJ, Yi C, Xu M, Wang JH, Liu YZ, Gao XC, Fu JW. Red to near-infrared electrophosphorescence from a platinum complex coordinated with 8-hydroxyquinoline. Appl Phys Lett 2006;89:233506.
[57] Shavaleev NM, Adams H, Best J, Edge R, Navaratnam S, Weinstein JA. Deep-red luminescence and efficient singlet oxygen generation by cyclometalated platinum (II) complexes with 8-hydroxyquinolines and quinoline-8-thiol. Inorg Chem 2006;45:9410–5.
[58] Niedermair F, Trattnig R, Mereiter K, Schmuck M, Sax S, List EJW, Slugovc C. Red electrophosphorescent platinum(II) quinolinolate complexes. Monatsh Chem 2010;141:847–58.
[59] Zhou CH, Zhao X. Theoretical investigation on quinoline-based platinum (II) complexes as efficient singlet oxygen photosensitizers in photodynamic therapy. J Organomet Chem 2011;696:3322–7.
[60] Lowe JA, Stacey OJ, Horton PN, Coles SJ, Pope SJA. Alkyl chain functionalised, cyclometalated platinum(II) complexes: syntheses, luminescence properties and X-ray crystal structure. J Organomet Chem 2016;805:87–93.
[61] Li XN, Feng JK, Ren AM, Li LJ. Theoretical studies of spectra properties of cyclometalated platinum(II) complexes with 8-hydroxyquinolines and quinolino-8-thiol ligand. Synthetic Met 2007;157:1046–53.
[62] Niedermair F, Kwon O, Zojer K, Kappaun S, Trimmel G, Mereiter K, Slugove C. Heteroleptic platinum(II) complexes of 8-quinolinolates bearing electron withdrawing groups in 5-position. Dalton Trans 2008:4006–14.
[63] Wu Y, Shan GG, Li HB, Wu SX, Ren XY, Geng Y, Su ZM. Theoretical study and design of multifunctional phosphorescent platinum(II) complexes containing triarylboron moieties for efficient OLED emitters. Phys Chem Chem Phys 2015;17:2438–46.
[64] Li ZM, Yuan JS, Ye YT, He YB, Huang B, Gao XC. 8-Hydroxy quinoline derivatives as auxiliary ligands for red-emitting cyclic-platinum phosphorescent complexes: synthesis and properties. Helv Chim Acta 2017;100:e1600308.
[65] Niedermair F, Sandholzer M, Kremser G, Slugovc C. Solution self-assembly and photophysics of platinum complexes containing amphiphilic triblock random copolymers prepared by ROMP. Organometallics 2009;28:2888–96.
[66] Ni J, Kang JJ, Wang HH, Gai XQ, Zhang XX, Jia T, Xu L, Pan YZ, Zhang JJ. A colorimetric/luminescent benzene compound sensor based on a bis(σ-acetylide) platinum(II) complex: enhancing selectivity and reversibility through dual-recognition sites strategy. RSC Adv 2015;5:65613–7.
[67] Ni J, Wang YG, Wang HH, Xu L, Zhao YQ, Pan YZ, Zhang JJ. Thermo- and mechanical-grinding-triggered color and luminescence switches of diimine-platinum(II) complex with 4-bromo-2,2'-bipyridine. Dalton Trans 2014;43:352–60.
[68] Gao LR, Ni J, Su MM, Kang JJ, Zhang JJ. Luminescence switching property of cycloplatinated(II) complexes bearing 2-phenylpyridine derivatives and the application for data security storage. Dyes Pigments 2019;165:231–8.
[69] Ghedini M, Pugliese T, La Deda M, Godbert N, Aiello I, Amati M, Belviso S, Lelj F, Accorsi G, Barigelletti F. Spectroscopy and electrochemical properties of a homologous series of acetylacetonato and hexafluoroacetylacetonato cyclopalladated and cycloplatinated complexes. Dalton Trans 2008:4303–18.
[70] Montes VA, Pohl R, Shinar J, Anzenbacher P. Effective manipulation of the electronic effects and its influence on the emission of 5-substituted tris(8-quinolinolate) aluminum(III) complexes. Chem Eur J 2006;12:4523–35.
[71] Sheldrick GM. SHELXS-97, Program for X-ray crystal structure determination. Germany: University of Gottingen; 1997.
[72] Sheldrick GM. SHELXL-97, Program for X-ray crystal structure refinement. Germany: University of Gottingen; 1997.
[73] Kalinowski J, Fattori V, Cocchi M, Williams JAG. Light-emitting devices based on organometallic platinum complexes as emitters. Coord Chem Rev 2011;255:2401–25.
[74] Ko SB, Park HJ, Gong SL, Wang X, Lu ZH, Wang SN. Blue phosphorescent N-heterocyclic carbene chelated Pt(ii) complexes with an α-duryl-β-diketonato ancillary ligand. Dalton Trans 2015;44:8433–43.
[75] Zhao JN, Kang H, Zhou SM, Sun HM, Yin SW, Zhao N, Tang BZ. Organic solid fluorophores regulated by subtle structure modification: color-tunable and aggregation-induced emission. Chem Sci 2017;8:577–82.
[76] Cui RR, Lv YC, Zhao YS, Zhao N, Li N. Solid-state fluorescent materials based on coumarin derivatives: polymorphism, stimuli-responsive emission, self-assembly and optical waveguides. Mater Chem Front 2018;2:910–6.
[77] Shigeta Y, Kobayashi A, Yoshida M, Kato M. Crystal engineering of vapochromic porous crystals composed of Pt(II)-diimine luminophores for vapor-history sensors. Cryst Growth Des 2018;18:3419–27.
[78] Shigeta Y, Kobayashi A, Ohba T, Yoshida M, Matsumoto T, Chang HC, Kato M. Shape-memory platinum(II) complexes: intelligent vapor-history sensor with ON−OFF switching function. Chem Eur J 2016;22:2682–90.
[79] Kobayashi A, Fukuzawa Y, Noro SI, Nakamura T, Kato M. Stepwise vapochromism observed for a simple terpyridine-platinum(II) complex with a thiocyanato ligand. Chem Lett 2009;38:998–9.
[80] Taylor SD, Norton AE, Hart RT, Abdolmaleki MK, Krause JA, Connick WB. Between red and yellow: evidence of intermediates in a vapochromic Pt(II) salt. Chem Commun 2013;49:9161–3.